Certification of Discontinuous Composite Material Forms for Aircraft Structures

Michael Roger Arce

A thesis

Submitted in partial fulfillment of the

Requirements for the degree of

Master of Science in Mechanical Engineering

University of Washington

2015

Committee:

Mark Tuttle, Chair

Ramulu Mamidala

Nathan Sniadecki

Program Authorized to Offer Degree:

Mechanical Engineering

Abstract

New, high performance chopped, discontinuous, or short fiber composites (DFCs), DFCs, such as HexMC and Lytex, made by compression molding of randomly oriented pre-impregnated unidirectional tape, can be formed into complex geometry while retaining mechanical properties suitable for structural use. These DFCs provide the performance benefits of Continuous Fiber Composites (CFCs) in form factors that were previously unavailable.

These materials demonstrate some notably different properties from continuous fiber composites, especially with respect to damage tolerance and failure behavior. These behaviors are not very well understood, and fundamental research efforts are ongoing to better characterize the material and to ease certification for future uses.

Despite this, these new DFCs show such promise that they are already in service in the aerospace industry, for instance in the Boeing 787. Unfortunately, the relative novelty of these parts means that they needed to be certified by “point design”, an excess of physical testing, rather than by a mix of physical testing and finite element analysis, which would be the case for CFCs or metals.

In this study, one particular approach to characterizing both linear-elastic and failure behaviors are considered. The Stochastic Laminate Analogy, which represents a novel approach to modeling DFCs, and its combination with a Ply Discount scheme. Owing to limited available computational resources, only preliminary results are available, but those results are quite promising and warrant further investigation.

Table of Contents

List of Figures

List of Equations

List of Tables

1. Introduction

The development and application of advanced composite materials in the aerospace industry and elsewhere have had a dramatic impact on the development of new product forms and technologies. Continuous fiber composites are extensively used to reduce the weight of finished products while maintaining strength. Continuous fiber composites are limited to specific product forms, as defined by the tape laying or filament winding procedures employed. As such, there are applications where a composite component could replace its metal counterpart, if the composite could be formed into the right geometry.

Enter a new class of advanced discontinuous fiber composite, under commercial names such as HexMC and Lytex, which aims to bridge the performance gap between unidirectional pre-impregnated (prepreg) carbon fiber reinforced polymer (CFRP) systems and traditional sheet molded compound forms. This allows for the performance improvements typical of composites as further weight reductions are realized when metal parts are replaced.

HexMC is an advanced discontinuous fiber composite system produced by compression molding of chopped prepreg CFRP. Carbon fiber prepreg is first cut into long strips,and then cut again into “chips”. The resulting chips are roughly 2” long and 0.33” wide. These chips are then consolidated together into new rolls, creating a secondary prepreg-like product form. This new system is then laid into matched metal compression molds and cured at high heat and pressure. Different prepreg precursor systems can be used to tailor the final properties; the HexMC material system used on the Boeing 787 is

comprised of AS4\8552 (1). Figure 1 shows a close up of the final material form. Note the appearance of randomly oriented chips and their distribution. The end result of this process is a new composite system whose elastic properties are similar to those of a quasi-isotropic system made from the same precursor; Figure 2 shows a normalized comparison of elastic moduli.

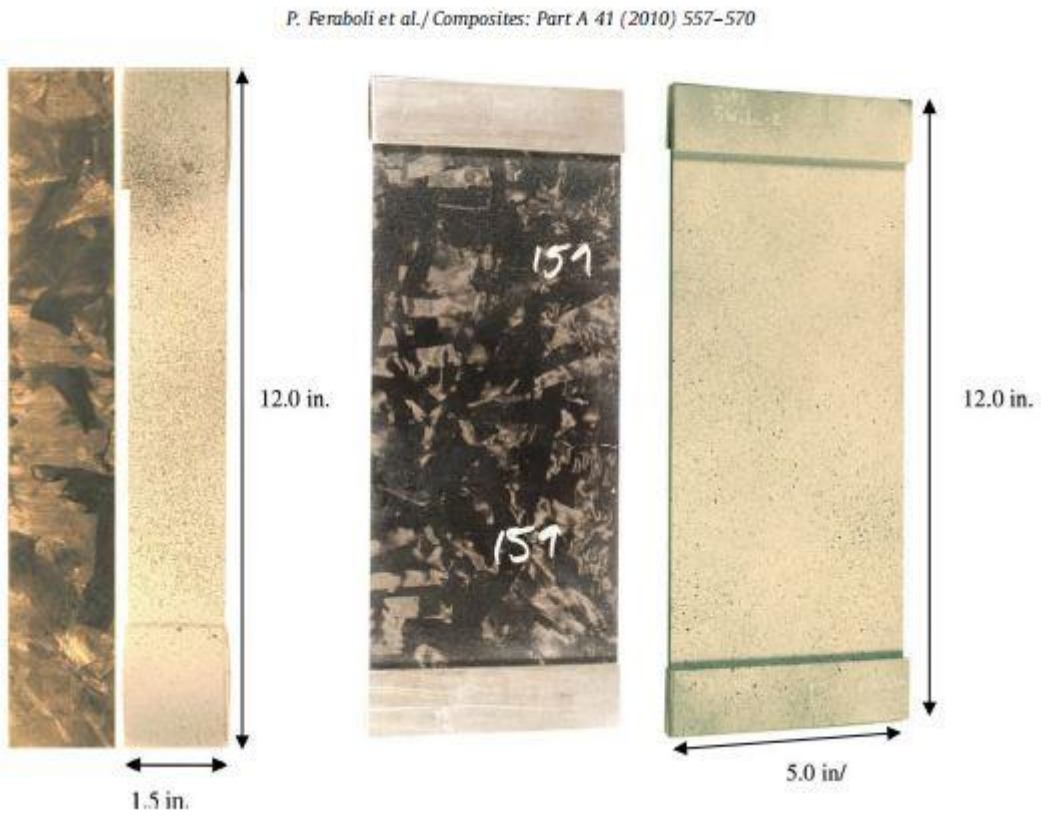

Figure 1: Close up of HexMC tensile coupons

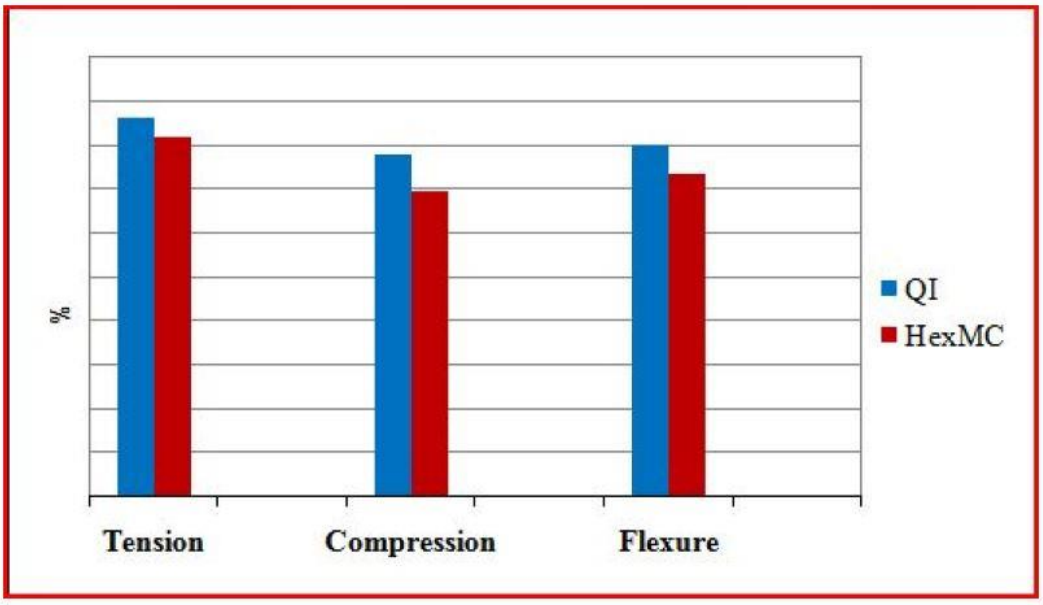

Figure 2: Normalized comparison of Elastic Moduli between HexMC and Quasi-Isotropic (QI) prepreg.

Compression molding allows for final shapes that are impossible to achieve using tape laying processes. In effect, DFCs of this nature allow properties similar to those of prepreg tape, but in a compression molded form. In addition to those gains, compression molding is also an inherently faster and higher volume process. Generally speaking, this allows the use of high performance DFCs where otherwise an aluminum part would be used, allowing the designer to meet design constraints while realizing the weight reductions associated with composite materials.

Owing to the non-uniform structure of these materials, as seen in Figure 1, they exhibit behaviors quite unlike those of CFCs. For example, the elastic modulus measured for HexMC exhibits a higher level of scatter than is typical of continuous-fiber composites, leading to failure mechanisms that are unlike those of CFCs. As such, applying existing

CFC structural analysis methods may result in overdesigned parts, and applying the same rejection criteria as CFCs during non-destructive testing leads to overly high DFC part rejection. (1)

As indicated, the damage tolerance, toughness, and failure behavior of the advanced DFCs are markedly different from their prepreg tape precursors. High performance DFCs exhibit apparent notch and defect insensitivity (2); where notched specimens of unidirectional CFRPs tend to fail in predictable ways, similar to isotropic materials, notched specimens of HexMC failed in seemingly random locations, and seemingly without regard for the notch.

Current certification efforts for composite systems in the aerospace industry don't translate readily to high performance DFCs due to these unusual properties. As such, certification in the past has been focused on "point-design" methods, wherein an abundance of physical testing is used to mitigate the lack of accurate FEA predictions.

HexMC, contrary to continuous fiber systems, shows itself to be relatively notch and defect insensitive. It is theorized that this behavior is due to the relatively high degree of modulus variation exhibited by high performance DFCs. Figure 3 shows the axial elastic modulus across two specimens during uniaxial testing via digital image correlation.

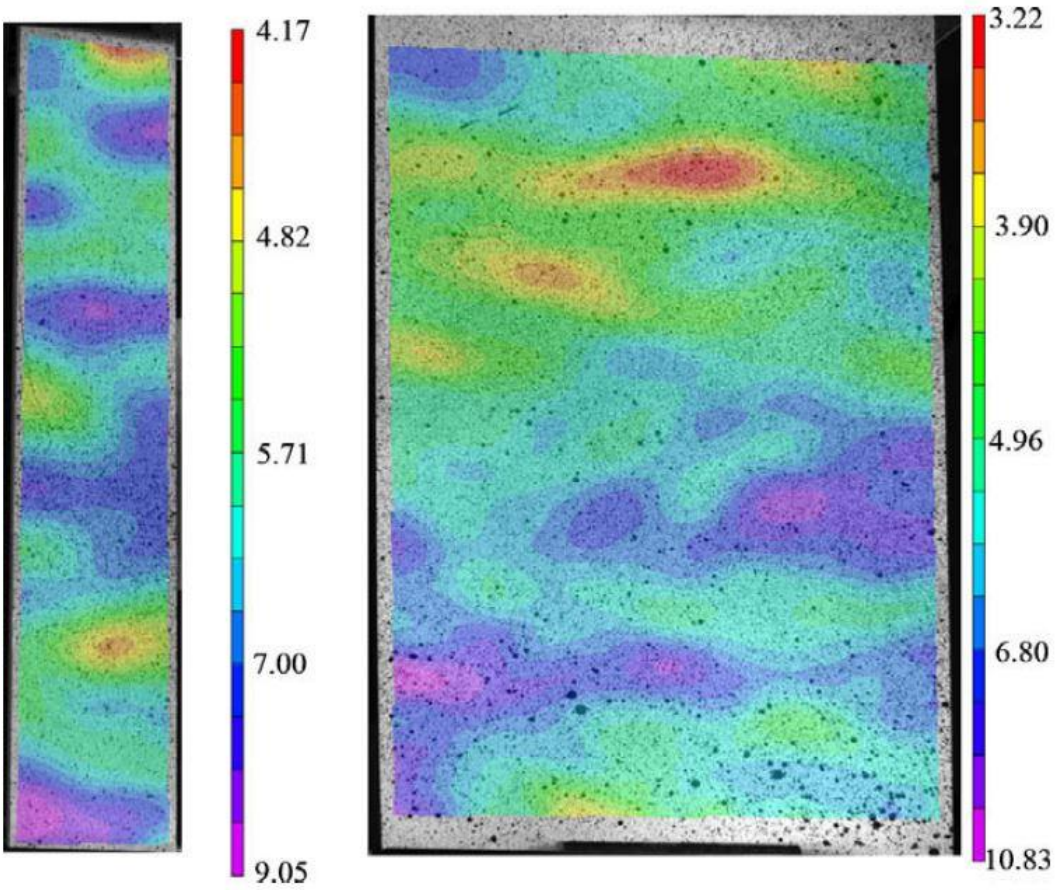

Figure 3: Variation in local Axial Elastic Modulus, Msi

A study (3) was performed by Hexcel, the manufacturer of HexMC, which ran a series of tests on specimens of DFC and CFC both derived from the same prepreg. The testing was done on pristine and damaged specimens, and it was found that while the CFC specimens showed the expected reductions in strength due to notches and damage, the DFC specimens showed essentially none. Figure 4 shows ultimate failure strengths for a base and a fatigued specimen of two different HexMC systems. Note that the fatigue samples failed within the same range as the base samples.

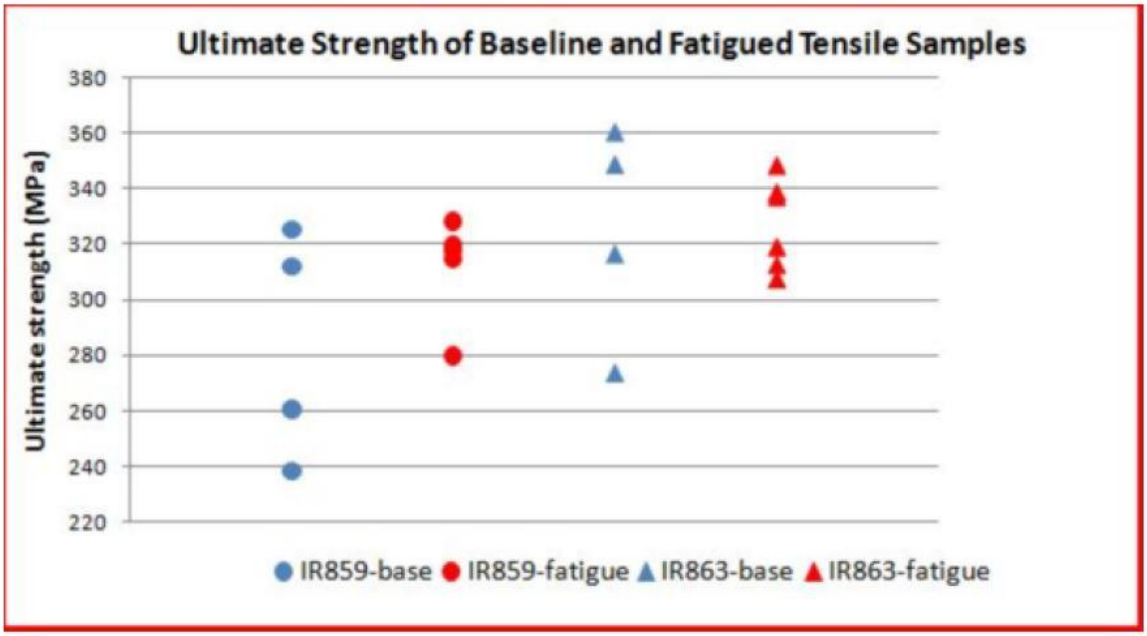

Figure 4: Comparison of UTS of base and fatigued DFC

Further investigation into the failure behavior of the material was performed. It was found that audible noise resulting from localized failure occurred at much lower load levels than for CFCs, but that such cracking did not indicate reduced strength of the overall structure. Indeed, post testing review via acoustic methods, liquid penetrant, and visual inspection revealed that such cracks were superficial, and rarely penetrated a significant distance into the thickness of the material.

Furthermore, the DFC exhibited excellent fatigue behavior, even relative to CFCs. The damage caused during testing did not seem to affect ultimate tensile strength of the DFC, as both fatigued and undamaged specimens showed the same variance.

2. Literature Review

2.1 B-Basis in modulus as well as strength

Traditionally, the aerospace industry uses the concept of B- Basis strength (4) as design parameters, where the B-Basis strength is the strength that is met or exceeded by 90% of specimens with 95% confidence. There are multiple methods of calculating these B-Basis values, and the value does depend on sample size, so more than one B-Basis value for a particular specimen is not uncommon. These parameters are used due to the inherent variability of real world materials, including for isotropic materials, and serve as a de facto additional factor of safety in structural design.

A previous investigation into HexMC led researchers at the UW to propose the extension of the A- and B-Basis ideas into moduli in addition to strength – in this manner, by performing a small number of deterministic tests using B-Basis properties one could produce a range of predicted load/displacement relationships within which HexMC parts could lie. This idea was investigated during the first phase of modeling the intercostal, and, as will be shown, has significant promise.

2.2 The Intercostal

Figure 5 shows an intercostal (HexMC door brace) is a HexMC product currently in service on the Boeing 787. It is a structural member that connects door frames to the fuselage. Many different configurations were produced for service in different areas of the plane, the specific part herein studied is depicted in Figure 5.

Figure 5: HexMC Intercostal

In the manufacture of the intercostal, at least two variations on the method are available; high flow versus low flow. In the former, the precursor material is placed mostly in the center of the mold and allowed to fill the model as it is heated. In the latter, the precursor material is spread more evenly within the mold, not spreading as much. These two approaches yield parts with slightly different properties, contributing to the range of behavior demonstrated, but due to limitations in modeling techniques, these differences were not considered in this study.

3. Hexcel Experiments

3.1 Experimental Set Up

In the tests performed by Hexcel, the intercostal was installed into a testing frame such that the flat region was bolted and held fixed, and the clip region was guided and not allowed to rotate or displace out of plane, shown in Figure 6. This set up does allow translation and rotation perpendicular to the long axis of the intercostal.

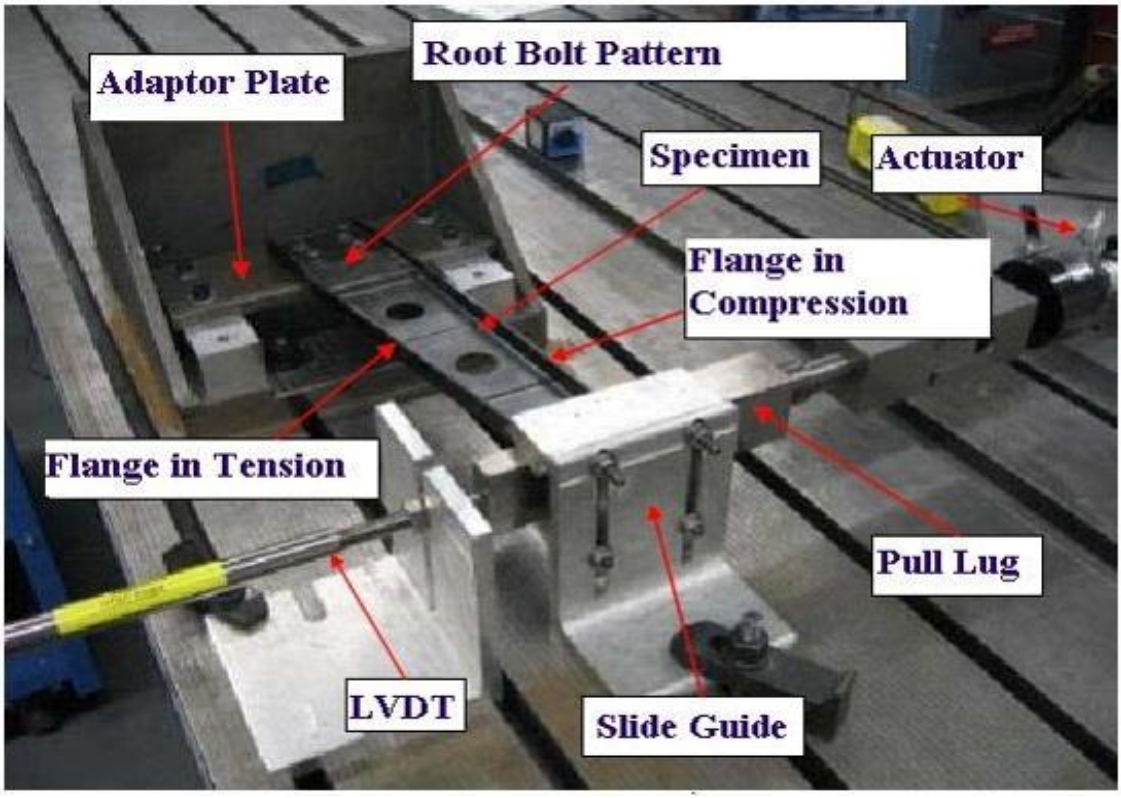

Figure 6: Hexcel Testing Frame

3.2 Testing parameters

Load was applied via a linear actuator which pulled on a plate to which the clip was bolted. This was an enforced displacement test, in which the actuator attempted to maintain a constant rate of displacement regardless of the amount of force required. For some of the specimens tested, the deflection was so great that an excessive tearing force presented at the clip face, which required the test be stopped, the specimen unloaded, and the rig reoriented such that the new position resulted in a force perpendicular to the clip face.

3.3 Results of the Hexcel Test Program

The specific results of Hexcel's testing are proprietary and are not detailed here. Of note is that the location in which failure occurred varied greatly over the 43 tests that were performed, rather than being localized to any one particular area of each specimen.

4. UW Experiments

4.1 Experimental Set Up

In the testing performed at the UW, the intercostal was installed into a testing frame such that the flat region was bolted and held fixed, and the clip region was allowed to rotate freely, as seen in Figure 7. A boss was bolted to the clip end, which was then loaded with a linear actuator connected by rope.

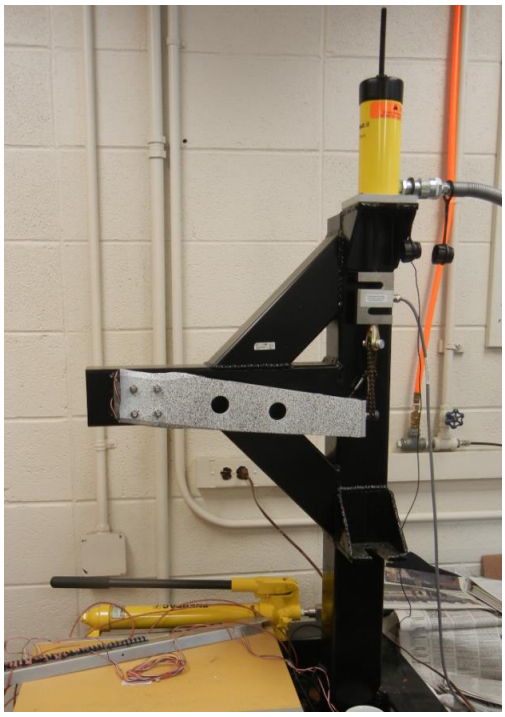

Figure 7: UW Intercostal Testing Rig

The first two tests had the DIC cameras set up to capture the entire clip end, while the last four tests had the DIC cameras set up to capture the top flange.

4.2 Testing parameters

The intercostal was initially loaded to 300 lbf and then relaxed to remove slack. The load was then steadily increased until it began to approach the range in which failure was expected to occur, at which point the load was increased in 5-10 lbf increments until failure occurred (5).

4.3 Results of our testing

In all six tests, failure was localized to the flange nearest the direction of loading, similar to the failure seen in Figure 8. It was for this reason that the DIC cameras were adjusted for the final two tests.

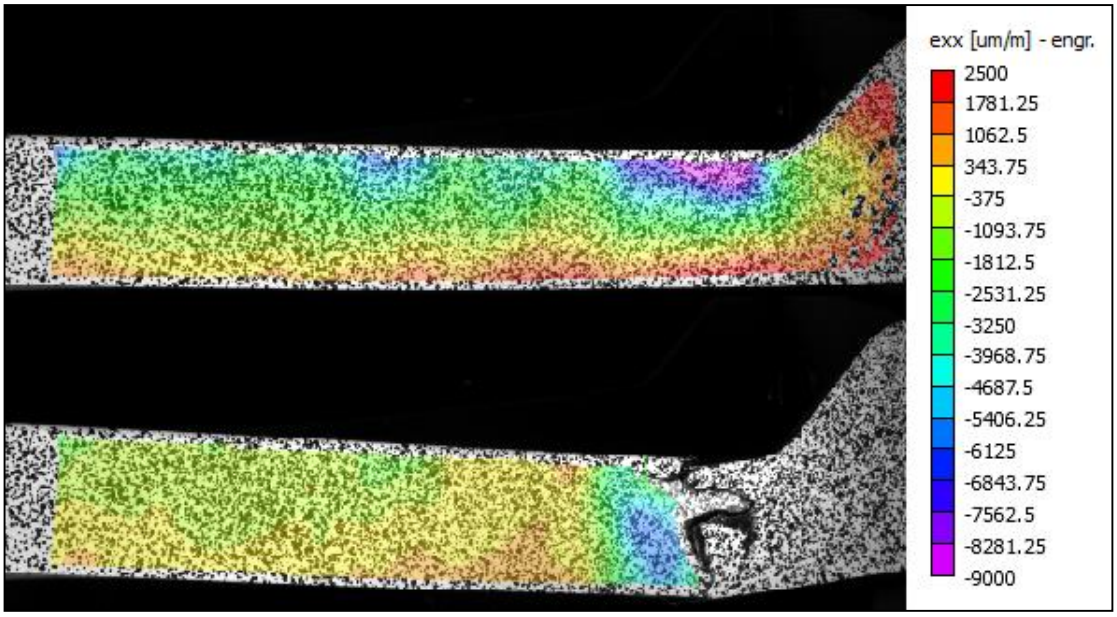

Figure 8: DIC Image of Failed Intercostal showing Principal Strain

It was speculated that allowing the clip end to rotate freely caused a significant stress concentration in the flange. This stands in sharp contrast to the Hexcel experiments, which, as previously stated, saw failure in many different locations.

5. The Stochastic Laminate Analogy

5.1 Motivation

As previously stated, HexMC exhibits a high degree of variability in material properties, and is considered "notch insensitive". As an attempt to capture this behavior, Feraboli et al (1) proposed the Stochastic Laminate Analogy (SLA), in which the material is considered as if it were a continuous fiber layup with random stacking sequences. Feraboli proposed that the randomized layups be confined to Random Representative Volume Elements (RRVEs), whose size would be determined via repeated finite element analyses, wherein each RRVE receives its own, unique random layup. Figure 9 contrasts RRVEs with the associated mesh.

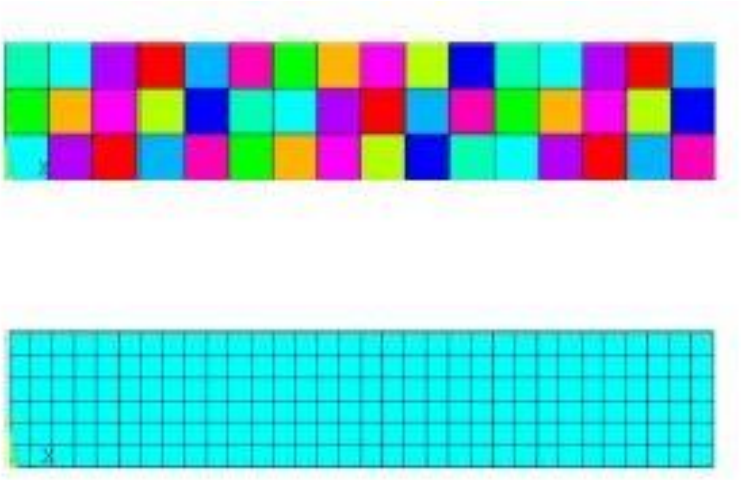

Figure 9: Representative regions (above), Finite Element Mesh (below) for a tensile coupon

Note that the random lay-up regions and mesh are independent of one another. This approach is stochastic in nature due to the randomization procedure, and as such a “large” number of analyses must be performed in order to produce useful information.

5.2 RRVE and sizing

Where Feraboli required that the stacking sequences were symmetric about the midplane, this condition was relaxed in subsequent work performed by Tuttle and Head (5). In order to signify this change, the RRVEs were renamed Random Laminate Volume Elements (RLVEs).

The size of the RLVEs was determined by minimizing the variation of elastic moduli over a large number of FEA analyses. Models were created with RLVEs of different sizes, and gauge regions were tracked during a series of analyses. Effective moduli were determined by dividing the strains in these regions by the nominal applied stress. The recommended RLVE size was that which gave the smallest standard deviation amongst these moduli - nominally squares 0.76” on a side.

5.3 Randomization

As stated above, each time a new analysis is performed, the layup within each RLVE is randomized using a random number generator. The angles are generated on a “ply by ply” basis and computed by multiplying a random number between 1 and 0 by 180° and subtracting 90° from the product, resulting in an angle between -90° and 90°. Figure 10 shows an example of a randomly generated layup.

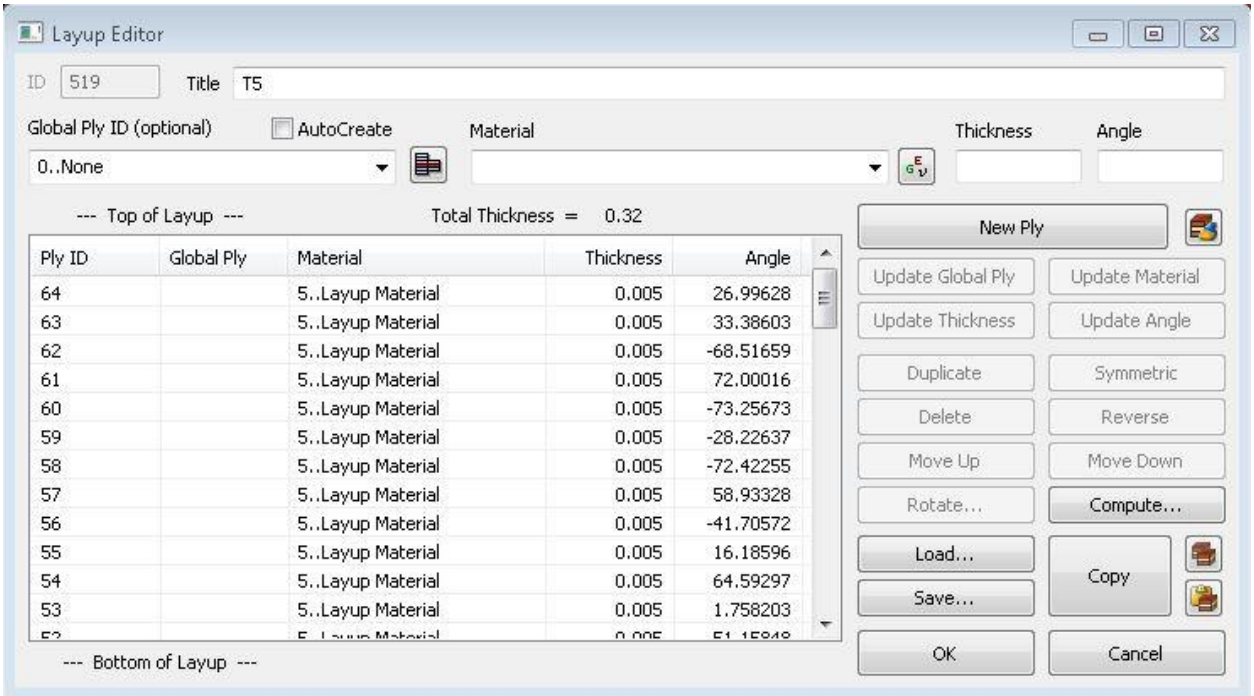

Figure 10: Layup Editor dialogue box, Femap v11.1.0

6. Femap Modeling

6.1 Hexahedral model

Hexahedral elements were initially used in an attempt to create a solid model. This turned out to not be feasible, as hexahedral elements require a more regular geometry than was present in the intercostal. In fact, the intercostal has many skewed angles, non-parallel line pairs, filleting, and chamfering, and various other non-uniform geometry elements so as to make hexahedral modeling very difficult if not impossible.

6.2 Mid-surface model

As an alternative method, a mid-surface model was created, wherein the intercostal was divided into a number of discrete regions, depending both on thickness and geometry, and each region was represented by 2d planes, rather than 3d solids. This also required

that the thickness changes present throughout were discretized into 6 distinct thicknesses, corresponding to 16 plies, 24 plies, 32 plies, 48 plies, and 64 plies. This represents an approximation when compared to the actual specimen, which had smooth thickness transitions. Figure 11 shows the now-discretized model, where the different colors represent different thicknesses.

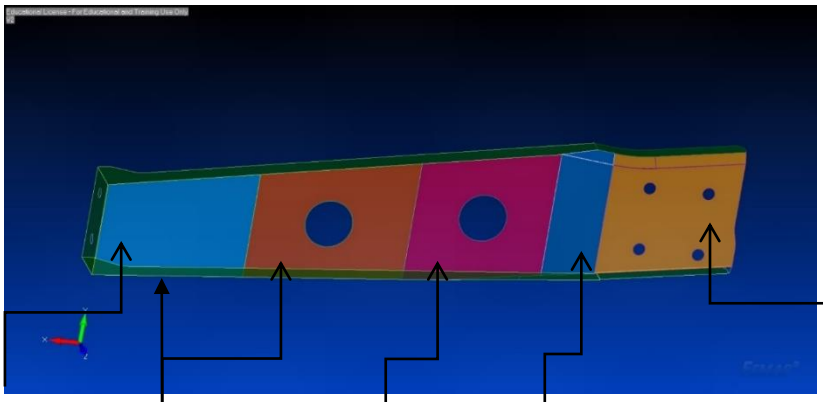

Figure 11: Discretized Intercostal Midsurface Model

Femap and NX Nastran use different terminology to refer to the same features, as Femap is designed to function with multiple pre- and post-processors. Three different element shapes were used, which in NX Nastran’s vocabulary are: CTRIA3, CQUAD4, and RBE2, indicating 3 node triangles, 4 node quadrilaterals, and rigid elements, respectively. The CTRIA3 and CQUAD4 elements were modified by a “pcomp” card, which made them laminate plate elements. The rigid elements are infinitely stiff connections used to bridge gaps present in the model due to the irregular geometry and thickness changes.

6.3 Software

Several commercially available programs were used in concert for this study. The modeling was carried out by Femap version 11.1.0, a pre- and post-processor usable with many FEA applications, in this case NX Nastran. The automation was carried out using Visual Studio 2013, a Windows-native integrated development environment, to interface with the Femap API, allowing a series of tasks to be carried out without further manual input. The results data from Femap were aggregated into Microsoft Excel, which was then used to create the various s and charts later presented.

7. Predicted Elastic response based on SLA

7.1 Nature of Analysis

The first set of analyses performed was to investigate the elastic response of the intercostal based on the SLA. This is done with two modeling approaches, one in which randomized properties are used in a "large" number of analyses, and a second where the various B-Basis properties are used in deterministic analyses. It is hypothesized that the results of the B-Basis properties will "bracket" those produced by the SLA analyses.

7.2 Material Properties

Two types of material properties were used: 2d Orthotropic and Isotropic. The 2d orthotropic material type was used to represent the chip level properties during the linear-elastic SLA, while the deterministic analyses used an isotropic material type to represent the B-Basis properties. The material properties used in the linear-elastic SLA analysis are sourced from (8). They are summarized in table 1.

Table 1: 2d Orthotropic Material Properties used in Linear Elastic SLA Analysis

E11 (Msi)	E22 (Msi)	G12 (Msi)	ν12
20.5	1.36	0.7	0.32

The B-Basis properties used for the isotropic, deterministic analyses are summarized in table 2. These values are sourced from (5).

Table 2: B-Basis Properties

Modulus (Msi)	B-Basis	Average	B-Max
Tension	5.58	6.62	7.65
Compression	5.36	6.31	7.27

7.3 UW Boundary Conditions

For the linear-elastic analyses, the inside curves of the four bolt holes at the bolt end were fixed, and a force per area totaling 200 lbf was applied to the clip end in the direction of loading. Figure 12 shows the UW boundary conditions used during the linear-elastic analyses.

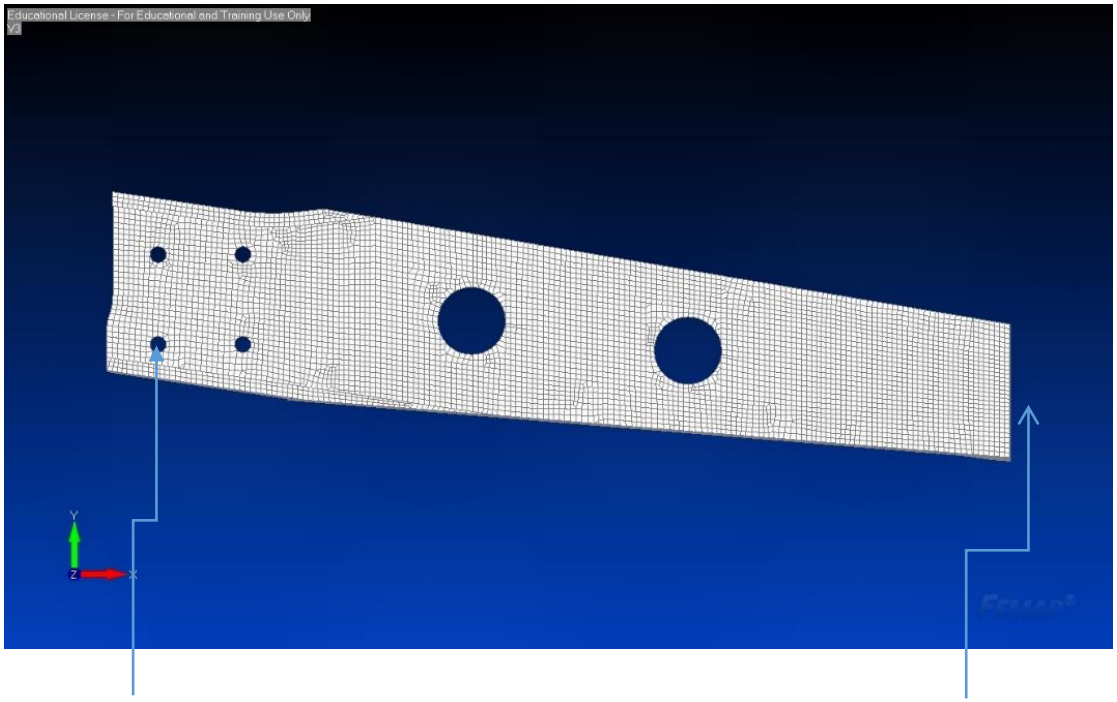

Figure 12: UW Boundary Conditions, Linear Elastic Testing

7.4 Results

The first analysis approach considered was a linear elastic test with loads within the linear region. Between each test, the fiber angles were randomized within each RLVE, such that each 24 second analysis generated a single pair of load/displacement values. This test was performed 1000 times with 1000 different layups. These tests were then compared against the results of deterministic tests using the B-Basis properties as

determined above. To form a basis of comparison, the deflections at a point of interest, node 6260, labeled in Figure 13, were monitored. When these deflections were divided by the applied load of 200 lbf, an effective stiffness can be obtained. It should be noted that while the twisting behavior depicted was indeed present, the deformation shown in Figure 13 is greatly exaggerated.

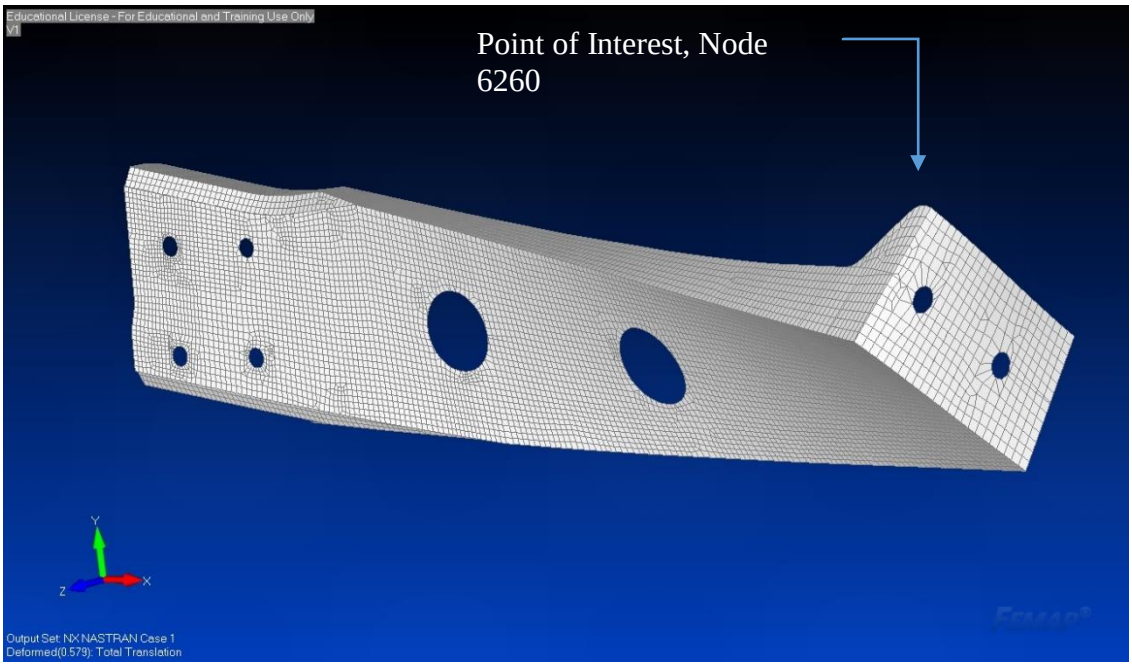

Figure 13: Point of Interest for UW Linear Elastic testing

Figure 14 below shows the results of the different B-Basis moduli run in the deterministic tests. The Tension and compression values are reported as solid and dotted lines respectively, while the maximum values are reported as diamonds, the average values reported as triangles, and the minimum values reported as squares.

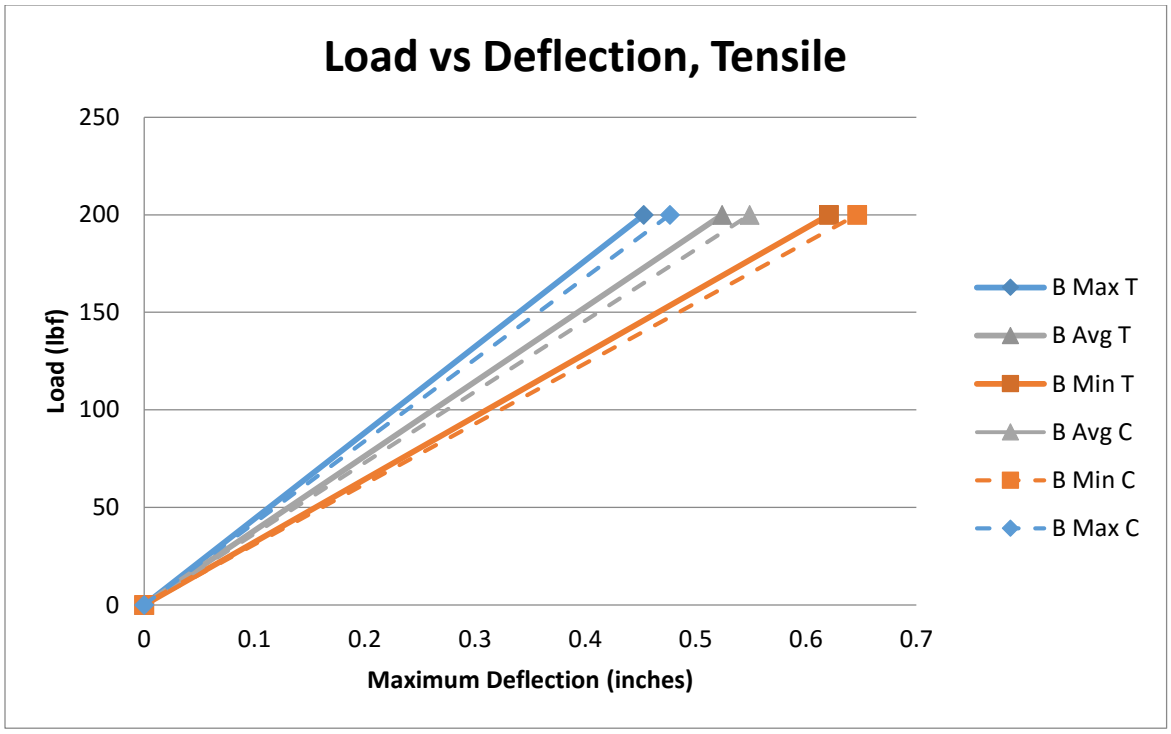

Figure 14: Deterministic Elastic Results

Owing to the nature of HexMC, there is not as much difference between the tensile and compressive properties as is typical of CFRPs. Figure 15 below shows the results of the 1000 SLA analyses superimposed on the deterministic results, where the SLA results are shown as yellow x-marks. Figure 16 presents the same data as a histogram.

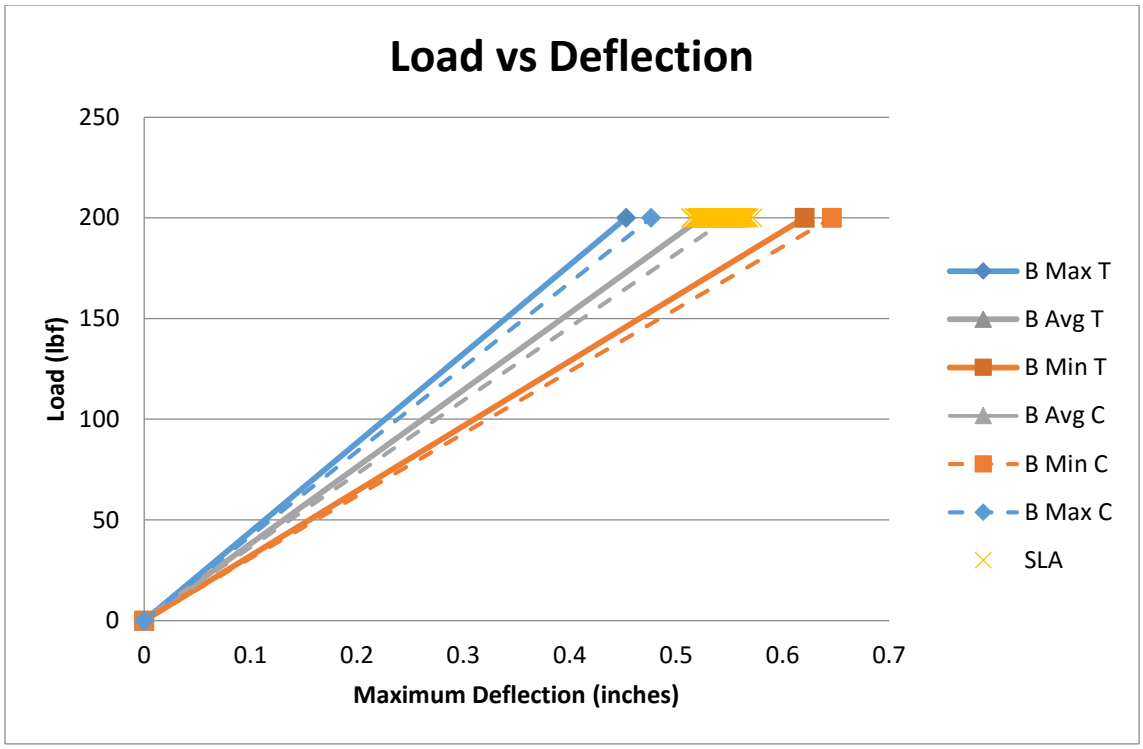

Figure 15: Deterministic and SLA Results Superimposed

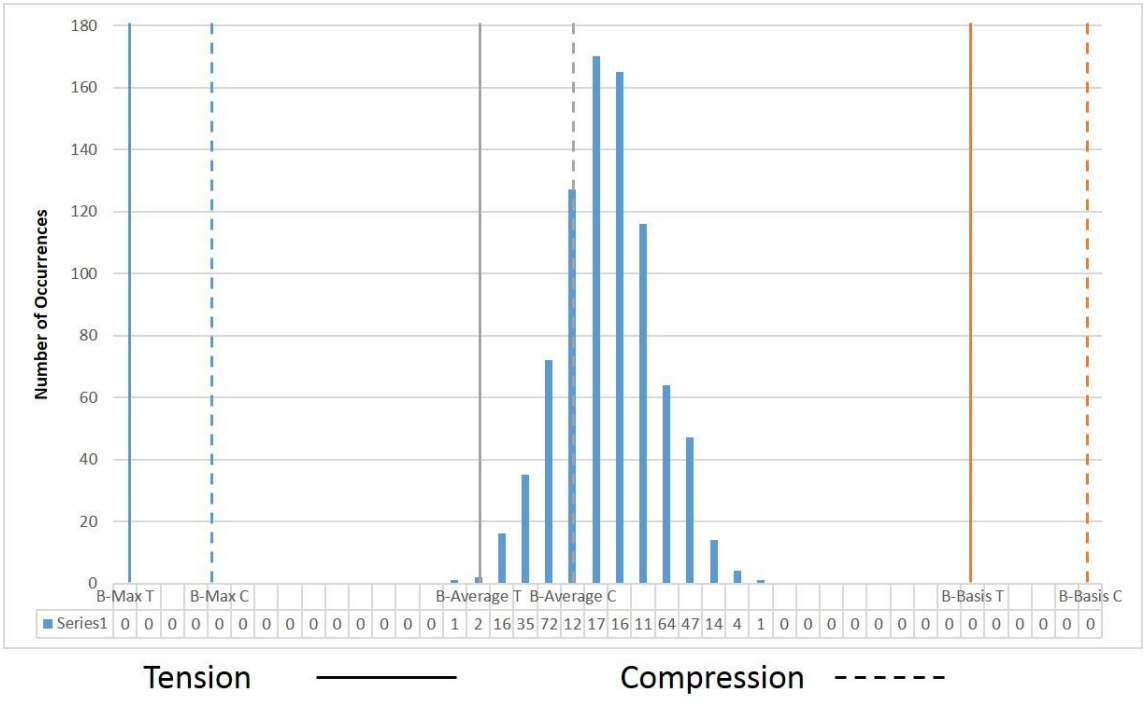

Figure 16: Histogram of SLA and Deterministic Superimposed

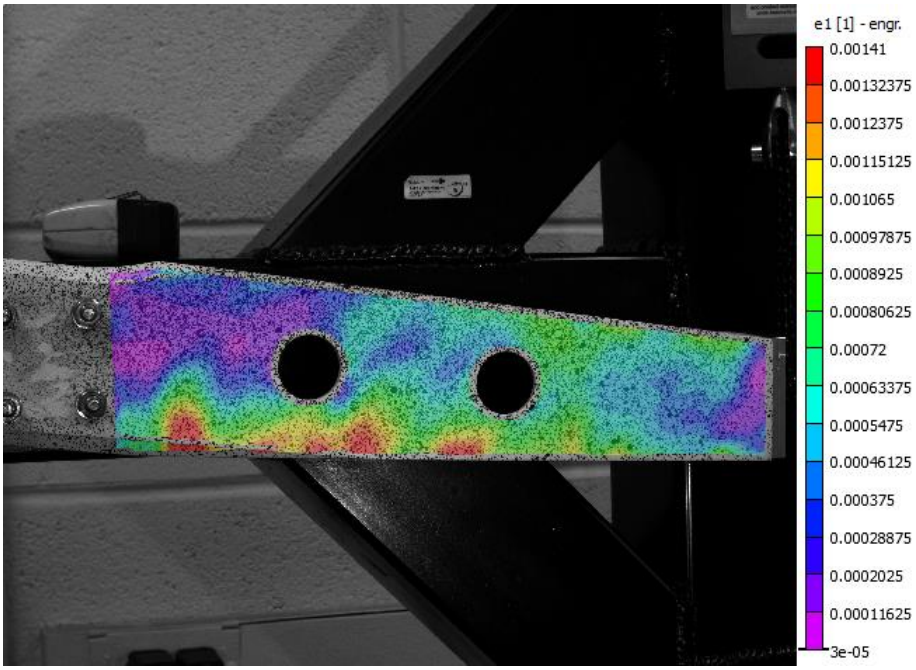

Figure 17: Typical DIC image, UW Experiment, Principal Strain

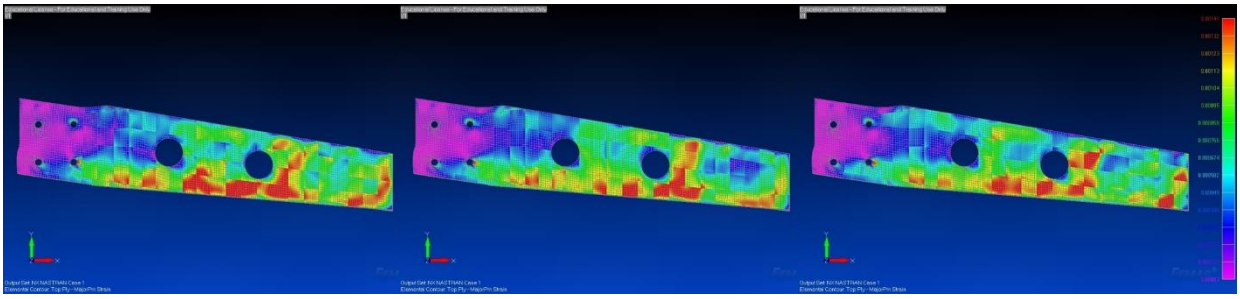

Figure 18: Typical Contour Plots of Principal Strain

Figure 17 shows a DIC image taken from experiments performed at the UW, while Figure 18 shows the results of three typical SLA analyses at the same load level. From left to right, the three images represent a relatively compliant, an average, and a relatively stiff stacking sequence.

7.5 Discussion

Figures 13 and 14 show that the SLA results fall quite close to the average B-Basis results. They are roughly centered about the compressive B-Average result and are slightly more compliant than the tensile B-Average result. While the SLA analyses consumed 25 hours of computing time, the deterministic analyses each took approximately 20 seconds. In this fashion, a designer could use the B-Basis properties and nearly immediately return a result that does indeed "bracket" the SLA results, as was expected. This result represents an opportunity to improve modeling efforts with little change in established methods. Additionally, Figures 16 and 17 largely show qualitative agreement between the strain patterns produced on the face of the intercostal between experiments and analyses. The strain field closest to the clip end is the most dissimilar between the experiment and analyses; this is due to an issue with the UW boundary conditions which is addressed in a later section.

8. Ply Discount Method

8.1 History and nature of the ply discount method

First proposed by Halpin, ply discount methods are meant to predict failure. As originally envisioned, ply discount scheme would be applied in a situation where there was a known set of experimental data to compare against. The comparison between the experimental data and the ply discount analysis would be used to fine tune the parameters used in the analysis.

Since it was proposed in the 1960's, the ply discount method has been one of several competing ideas on how to approach failure in composite materials. Compared to some

other such ideas, the ply discount scheme has the advantage of being based on Classical Lamination Theory (CLT), meaning it can be readily incorporated into common FEA programs without the need for special tools to handle sub-ply level behavior. Conversely, CLT relies upon the Kirchhoff Hypothesis (10), which states that “a straight line which is initially perpendicular to the midplane of the plate remains straight and perpendicular”. Owing to the nature of damage propagation within advanced composite materials, as more and more damage occurs, the Kirchhoff Hypothesis becomes less and less valid.

8.2 Unit Loads, Enforced Displacements

Basically speaking, a ply discount method is an approach where a failure criterion is used to determine a critical region of the specimen, determine the load required to cause failure, reduce the material properties at that location, enforce the displacement corresponding to the failure load, and record the resulting constraint force corresponding to that displacement. If this second analysis on the now weakened structure results in the failure criterion being met again, the process is iterated until no new ply failures occur. At that point, a new unit load is applied, and the process begins again, running in this fashion until a predetermined Final Fracture criterion has been met. Figure 19 shows a flow chart of this process.

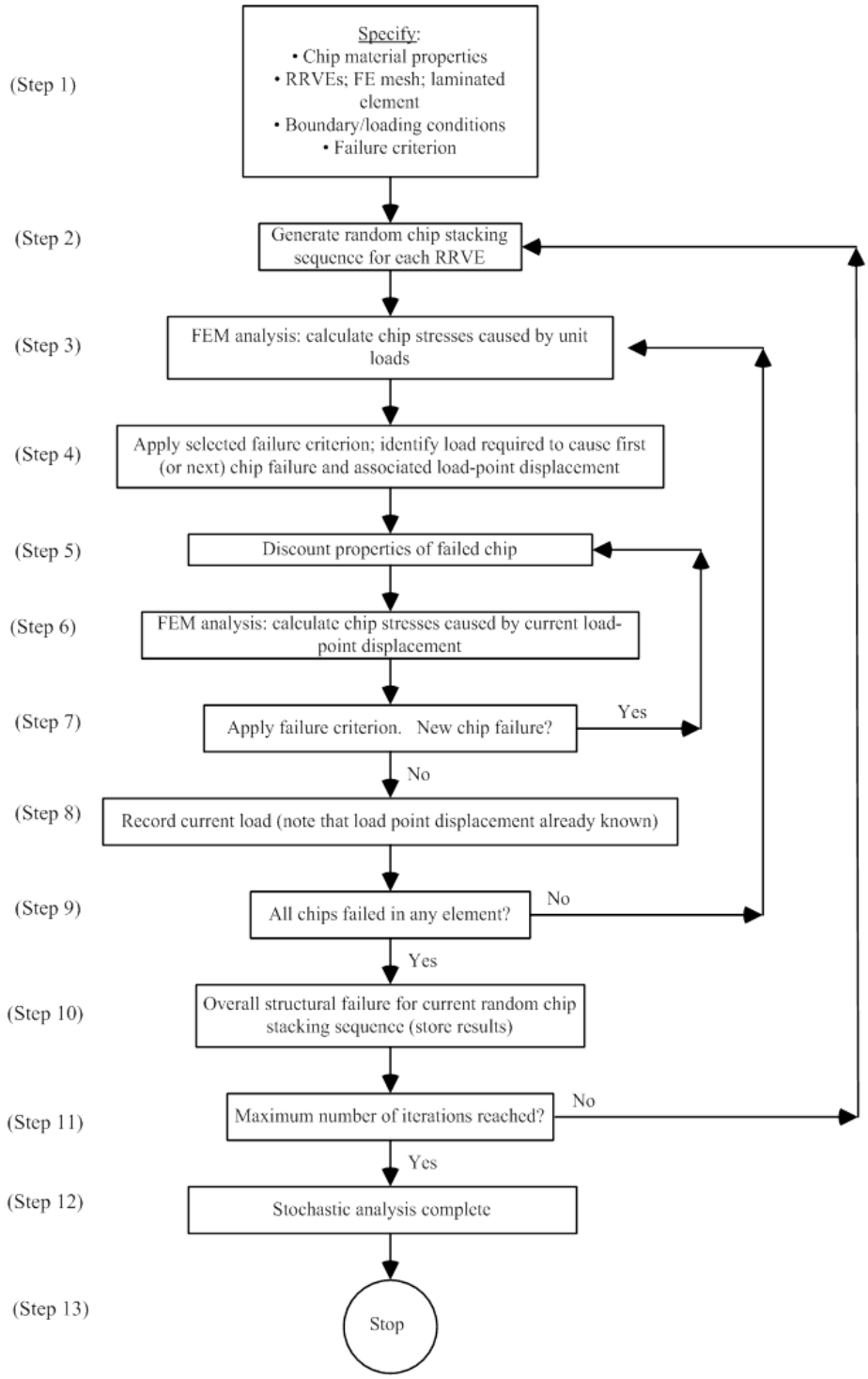

Figure 19: Ply Discount Scheme Flow Chart

8.3 Ply Failure Criterion

For these analyses, a failure criterion suitable for composite materials is required. In the present analysis, the Tsai-Wu criterion, equation 1, was chosen. X_1, X_2, X_{11}, X_{22}, and X_{66} are parameters based on the ratio of the tensile and compressive strengths for the 1 and 2 directions. There is no widely accepted method by which to calculate the parameter X_{12}; herein it is calculated as negative one half the square root of the products of all four failure strengths. The basis of this choice is that when operated with isotropic strengths, the Tsai-Wu criterion reduces to the familiar Von Mises criterion used for isotropic materials. Further details are available at (10).

Equation 1: Tsai-Wu Failure Criterion for plane stress

$$X_1\sigma_{11} + X_2\sigma_{22} + X_{11}{\sigma_{11}}^2 + X_{22}{\sigma_{22}}^2 + X_{66}{\tau_{12}}^2 + 2X_{12}\sigma_{11}\sigma_{22} < 1$$

A load factor, L, is then introduced as a unit-less factor attached to every stress term.

$$X_1(L\sigma_{11}) + X_2(L\sigma_{22}) + X_{11}(L\sigma_{11})^2 + X_{22}(L\sigma_{22})^2 + X_{66}(L\tau_{12})^2 + 2X_{12}(L\sigma_{11})(L\sigma_{22}) = 1$$

Equation 2: Rearranged Tsai-Wu Criterion

$$L^2(X_{11}{\sigma_{11}}^2 + X_{22}{\sigma_{22}}^2 + X_{66}{\tau_{12}}^2 + 2X_{12}\sigma_{11}\sigma_{22}) + L(X_1\sigma_{11} + X_2\sigma_{22}) - 1 = 0$$

The quadratic equation can then be used to solve for L, which corresponds to the load required to cause first ply failure.

8.4 Ply Discount Constants

The material properties broken into fiber dominated properties, such as E_{11}, and matrix dominated properties such as E_{22} and the shear moduli. These properties are reduced by different degrees during the course of the analysis. There are no universally accepted values for these ply discount constants (11) – as originally proposed, the modeler would

choose these values to best match experimental results on a case by case basis. As a starting point, fiber dominated properties were reduced to 70%, and the matrix dominated properties were reduced to 30%

8.5 Concluding the Analysis: Structural Fracture Criterion

The process is iterated many times. Each time, the properties of an individual ply within the element that has failed are discounted, reducing the fiber dominated properties and the matrix dominated properties by a set of constants. Eventually, an individual element within the model will have all of its plies failed. As a starting point, this is considered a structural fracture, and at this point, the analysis ends. As will later be seen, this is found to be too conservative a fracture criterion and alternatives are discussed in the following section.

9. SLA-PD As Applied to the Intercostal

9.1 Material Properties

When classical lamination theory is applied to an isotropic layup with the properties of AS4/8552 it predicts elastic properties that are about 18% higher than those reported for HexMC. As a result, the values used for the 2d orthotropic material properties were adjusted downward until they matched the values Classical Lamination Theory (CLT) predicted would result in the elastic properties reported for HexMC. The elastic properties utilized in the analysis are summarized in Table 3.

Table 3: Reduced Material Properties used in the SLA-PD Analysis

E_{11} (Msi)	E_{22} (Msi)	G_{12} (Msi)	ν_{12}
17.1	1.16	0.646	0.32

Additionally, table 4 summarizes the failure strengths used in the SLA-PD analysis. Again, these values were obtained via CLT after adjusted the orthotropic properties downward.

Table 4: Failure Strengths used in the SLA-PD Analysis

σ_{1t} (Ksi)	σ_{1c} (Ksi)	σ_{2t} (Ksi)	σ_{2c} (Ksi)	τ_{12} (Ksi)
147	137.8	5.375	6.89	7.626

9.2 Hexcel Boundary Conditions

The boundary conditions considered for the Hexcel tests were similar to the initial approach to the UW boundary conditions, except that for the Hexcel testing, the clip end was only allowed to translate in the direction of loading; it was not allowed to translate out of plane or rotate in any direction. Figure eight in section 3.1 shows the Hexcel testing frame.

Figure 20 shows the boundary conditions used to simulate this set up. As before, the inside curves of the bolt holes are fixed, but in this case the nodes around the perimeter of the clip end are constrained such that they may move only in the direction of loading.

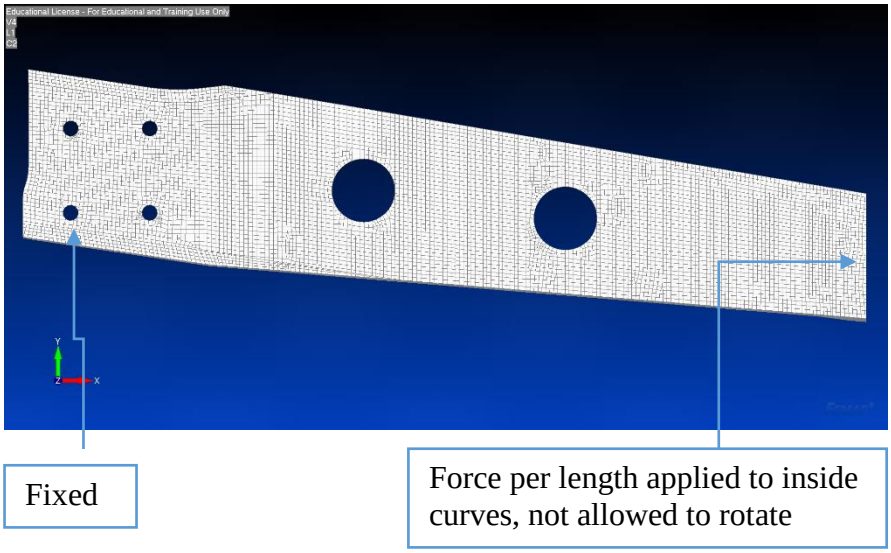

Figure 20: Hexcel Boundary Conditions

9.3 Revision to UW BCs

A meeting was held with Hexcel after the linear-elastic SLA results were presented at the JAMS in Spring 2014. From discussion regarding boundary conditions at that meeting, it was found that the boundary conditions applied are not the best way to represent the damage patterns produced by UW testing. As a result, instead of a force per area applied to the clip face, a new node was created which represents the center of the boss attached to the clip end, which is the new point of loading, presented in Figure 21. The plate was represented by creating rigid connections from that new node to the nodes on the clip face. As before, the clip end is allowed to rotate freely.

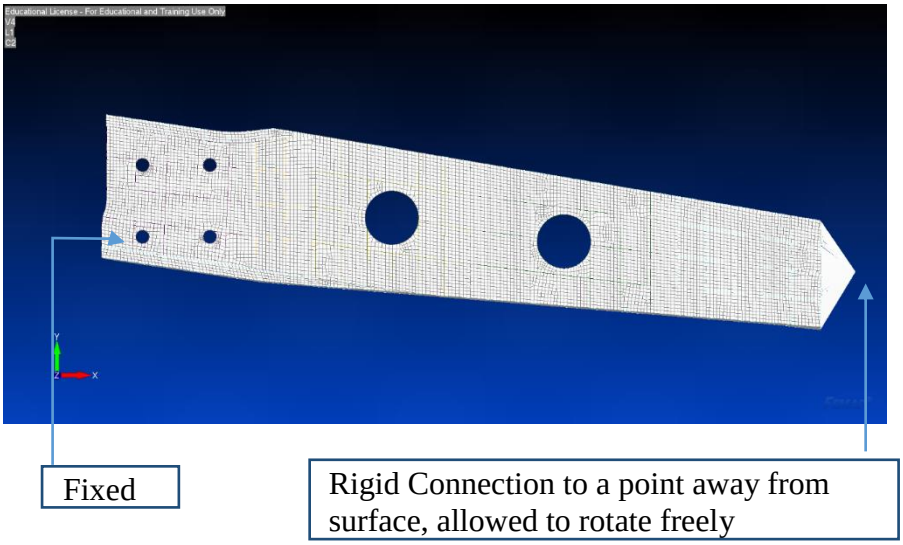

Figure 21: Revised UW Boundary Conditions

9.4 Ply discount constants and the change

For this analysis, two different sets of constants were considered, one where the fiber dominated properties were reduced to 70%, and the matrix dominated properties were reduced to 30% and the second with the fiber dominated properties reduced to 60% and matrix dominated properties reduced to 1%. As will be seen, both sets return approximately the same results, but the latter set results in reduced analysis times. This is because the vastly weaker matrix properties tend to direct the load path to a greater degree.

9.5 Structural Fracture Criterion

As previously stated, there is no obvious, decided-upon, structural failure. As such, three separate structural fracture criteria were considered, a) when a single element has all its plies failed, b) when a number (e.g. 10) elements have all their plies failed, and finally c) where the stiffness of the overall structure (as represented by Applied Load / Deflection) has reduced to 90% of its original value. The results returned by cases a) and b) proved to be quite similar to each other, and so the results of case b) are only briefly summarized. In this model, there are a total of 8009 laminated elements. When operated through with the corresponding number of plies per element, a total of 250,200 “ply” failures are possible.

9.6 Results for One element failure

Table 5 summarizes the results of the SLA-PD analyses for the UW boundary conditions. As can be seen, analysis times varied, but generally last about 9 hours.

Table 5: SLA-PD Results, UW BCs, One Element Failure

Analysis	Number of Ply Failures	Load at Failure	Time
1	942	339.62	10 H, 40 M
2	765	397.41	8 H, 45 M
3	872	494.21	9 H, 10 M
4	620	397.85	7 H, 10 M

Figure 21 shows the load displacement relationship at the point of loading. The range of stiffnesses present in the intercostal is represented by the different slopes of each data set. In this load range, the relationship is essentially linear, with very slight aberrations. Figure 22 shows the same data at an expanded scale, where it is clear that these aberrations represent the drop in load required to maintain a particular displacement as the model is being damaged. The thick blue vertical line is actually a series of data points that are so tightly clustered they appear as a line. It stands to reason that each successive damaged ply causes so small a reduction in load, as each individual ply is a very small part of the overall model.

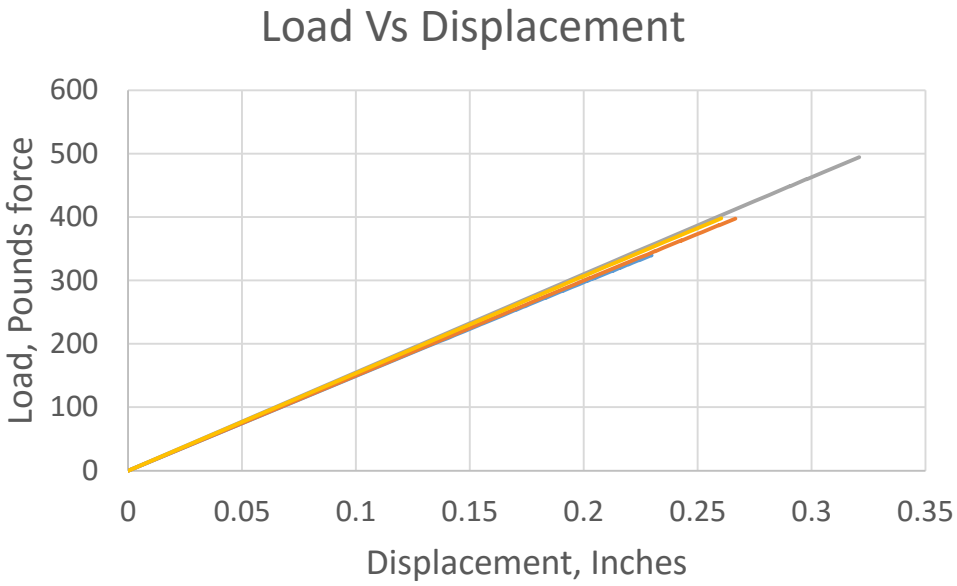

Figure 22: SLA-PD, UW BCs, Load vs Displacement

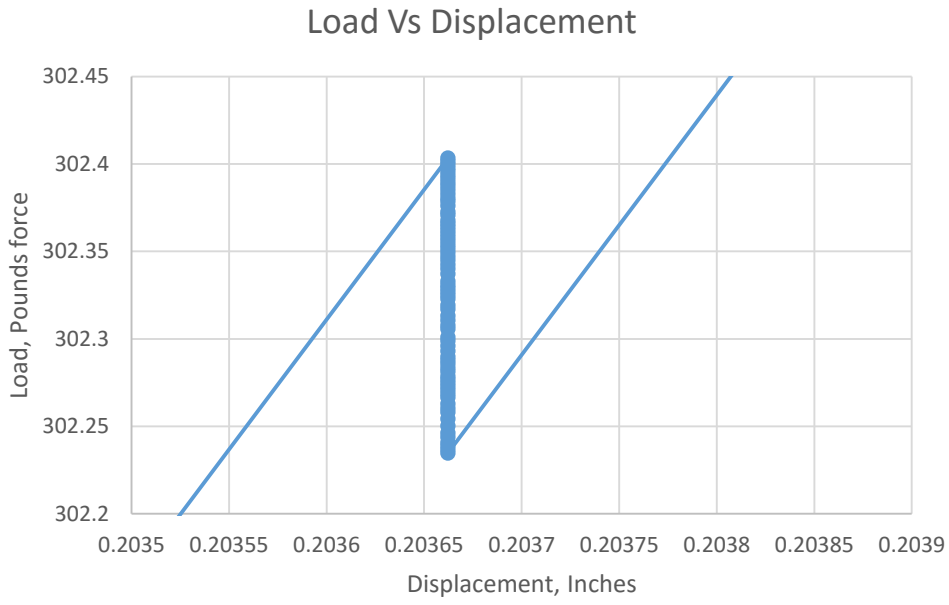

Figure 23: SLA-PD, UW BCs, Load vs Displacement, Expanded Scale

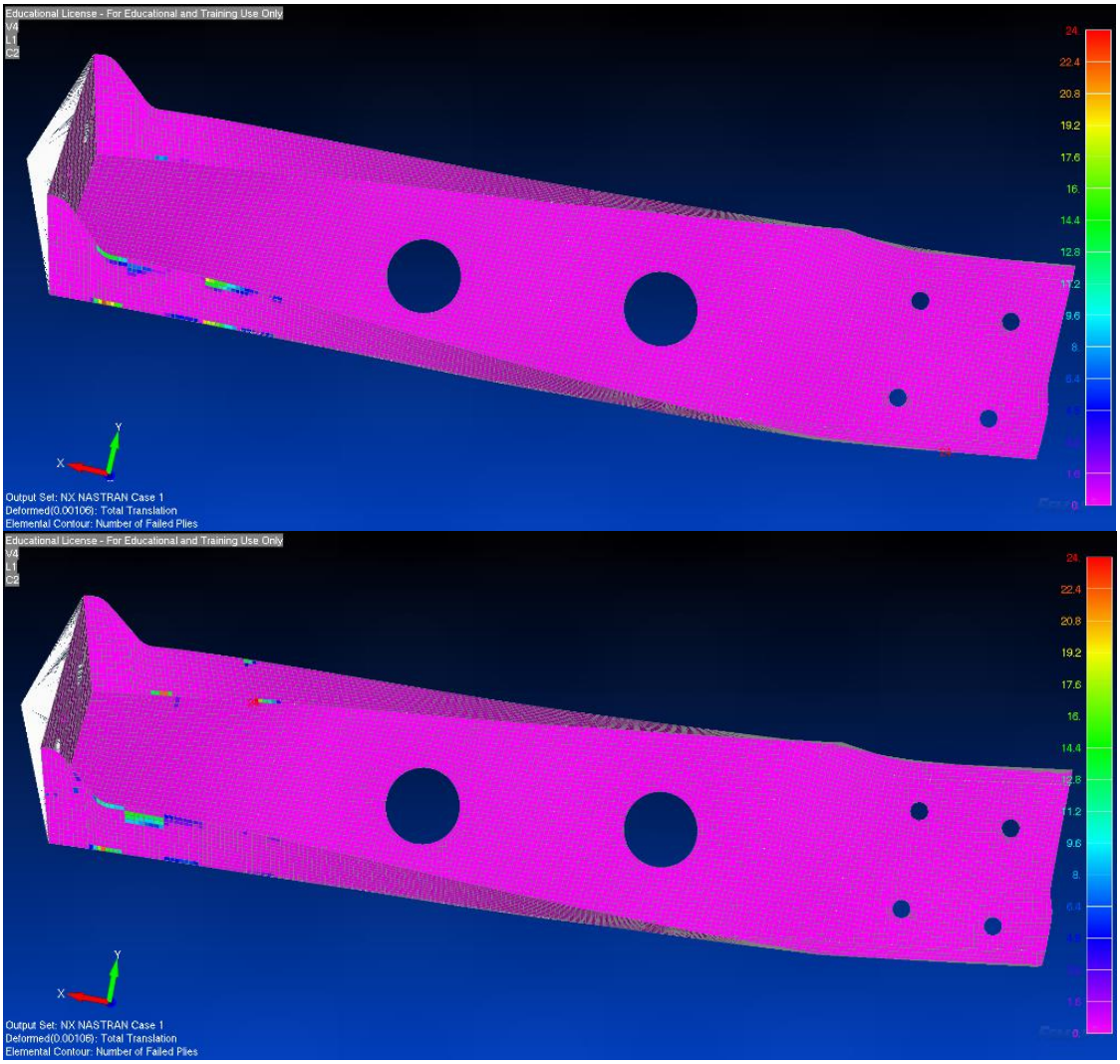

Figure 24: Typical SLA-PD Damage Patterns, UW BCs, One Element Failure

Figure 23 shows two typical damage patterns corresponding to UW BCs and one element failure. As expected, damage is localized almost exclusively to the flanges at the clip end. This is consistent with the experiments performed at the UW, where failure occurred in the same region each time.

Table 6: SLA-PD Results, Hexcel BCs, One Element Failure, Normalized

Analysis	Number of Ply Failures	Load at Failure	Time
1	1079	0.864332	5 H, 40 M
2	3900	0.998955	20 H, 40 M
3	3514	1	18 H, 50 M
4	1555	0.909943	8 H, 35 M
5	1787	0.947572	9 H, 50 M
6	1699	0.934449	9 H, 20 M
7	1621	0.867419	9 H, 5 M
8	792	0.742157	4 H, 45 M
9	2315	0.878562	12 H, 35 M
10	1240	0.800165	7 H, 20 M

Table 6 summarizes the ten completed analyses using Hexcel boundary conditions. As with the UW results, analysis times varied. Here the average was a bit higher at roughly 10.5 hours.

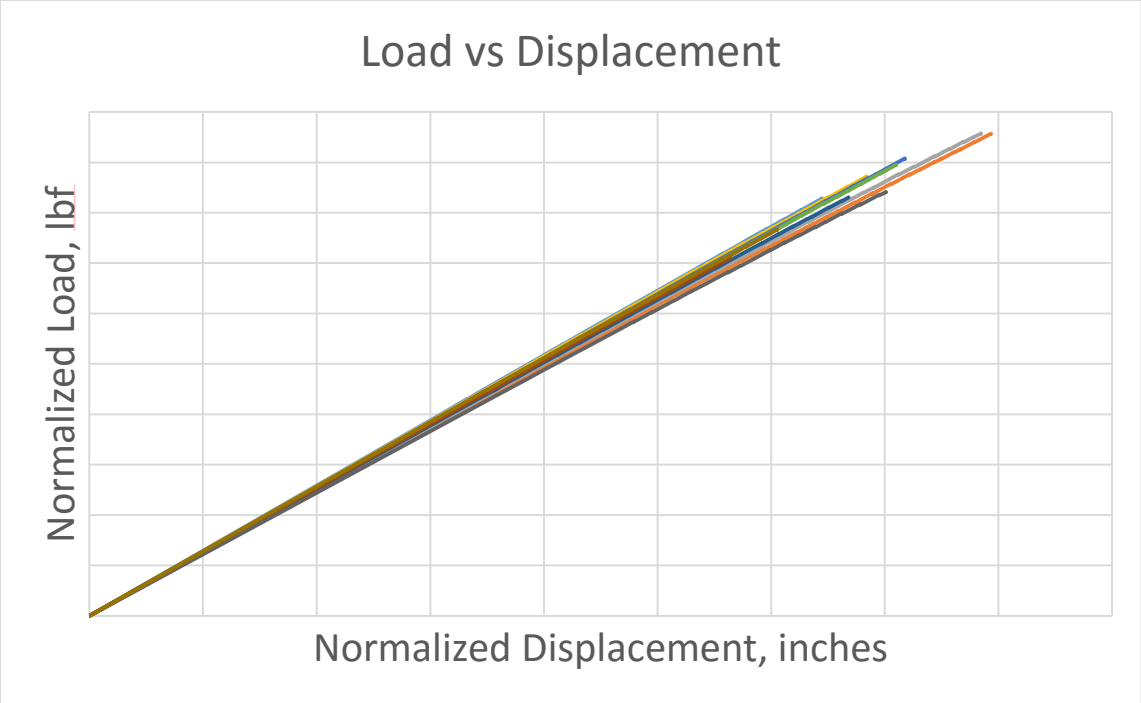

Figure 25: SLA-PD, Hexcel BCs, Load vs Displacement, Normalized

Figure 25 shows the load displacement relationship for the Hexcel boundary conditions. As before, the range of stiffnesses present in the intercostal is represented by the different slopes of each data set. Figure 26 shows typical damage patterns for the Hexcel boundary conditions. In this case, damage is far more distributed about the model than in the former case, consistent with experimental observations by Hexcel, where, again, it was found that failure occurred in many different locations, rather than being localized to one area as in the UW experiments.

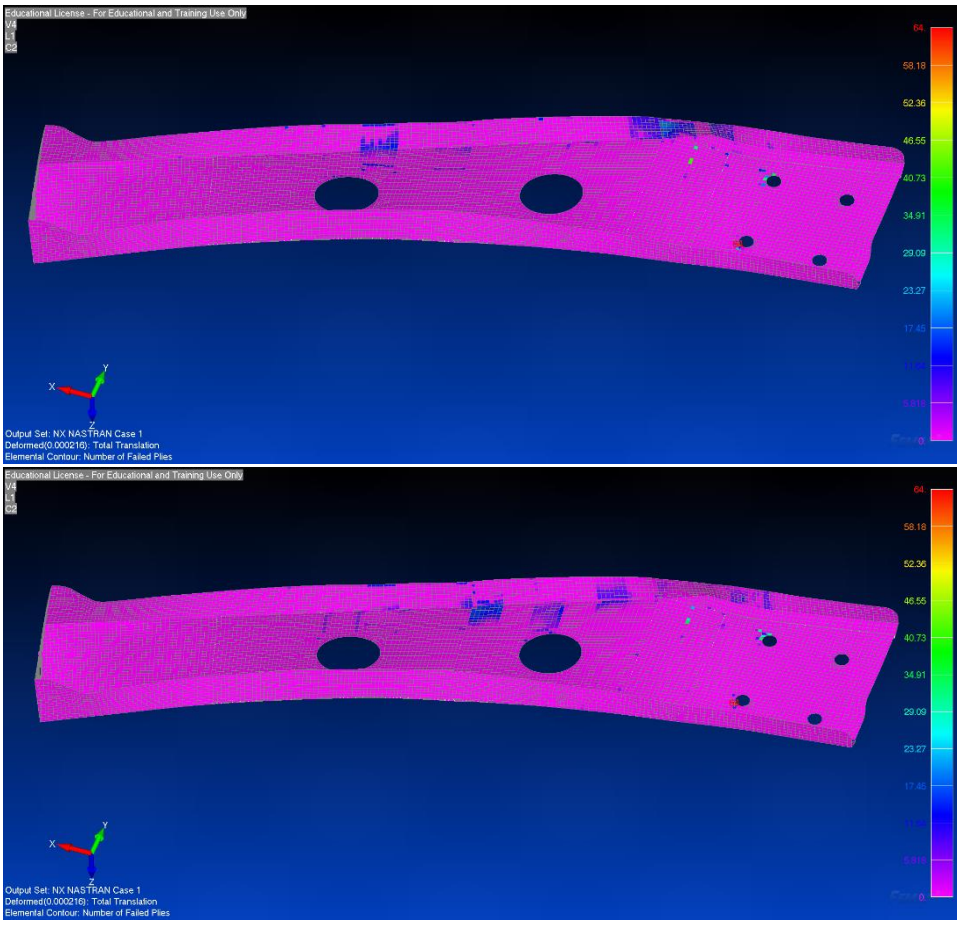

Figure 26: Typical SLA-PD Damage Patterns, Hexcel BCs, One Element Failure

9.7 Discussion for One Failed Element

For both sets of boundary conditions, the damage patterns predicted by the analysis were consistent with the damage observed during the respective experiments. The amount of damage, however, seems to correspond to miniscule tears, rather than structural failure of the part as a whole; this indicates the analysis has ended prematurely and that a new structural fracture criterion is required.

9.8 Results for 10% Stiffness Reduction

Table 7: SLA-PD Results, Hexcel BCs, 10% Stiffness Reduction

Analysis	Number of Ply Failures	Load at Failure	Time
1	10872	1	49 hrs 30 min
2	8766	0.949042	41 hrs 20 min
3	8641	0.934321	44 hrs, 20 min

Table 7 summarizes the results of the 90% stiffness criterion with Hexcel boundary conditions. Comparison of tables 6 and 7 immediately reveals a massive increase in analysis time, going from an average of 10 hours to an average of 45 hours. This is because the 90% stiffness criterion requires many more iterations, resulting in upward of 50 fully failed elements, as opposed to only one.

Figure 27 shows the load-displacement relationship for the 90% stiffness criterion and the Hexcel boundary conditions. As opposed to Figure 25, this Figure shows some nonlinearity as load is further increased. In this fashion, the SLA-PD analysis simulates a non-linear finite element analysis. Figure 28 shows the overall stiffness of the intercostal plotted against the number of ply failures. In this case too, the variation in the lines shows the scatter of effective properties.

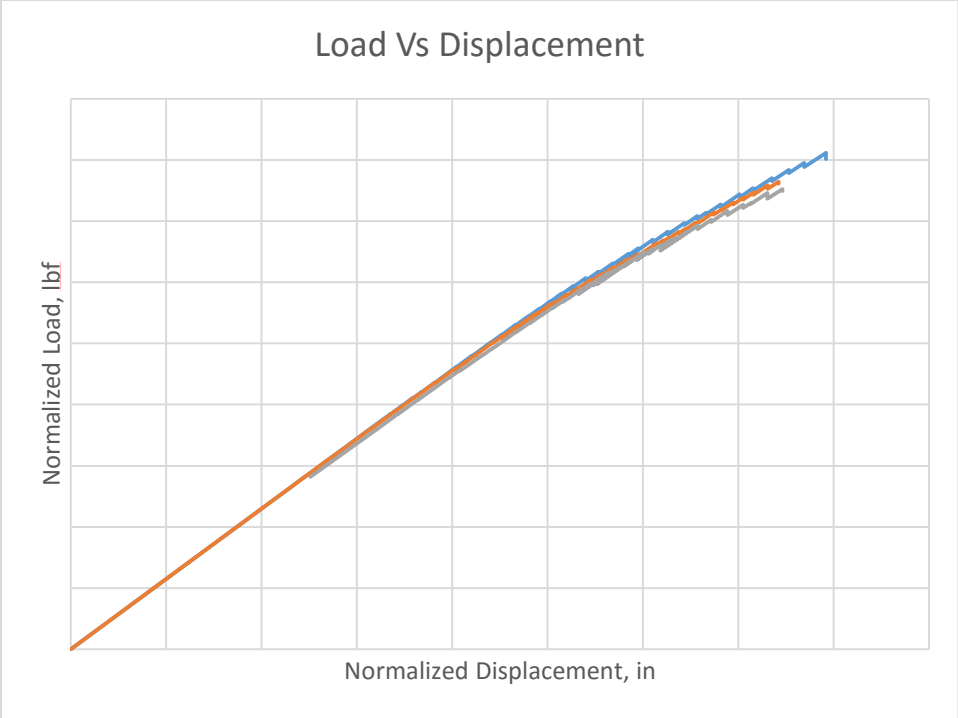

Figure 27: SLA-PD Results, Hexcel BCs, Load vs Displacement, 10% Stiffness Reduction, Normalized

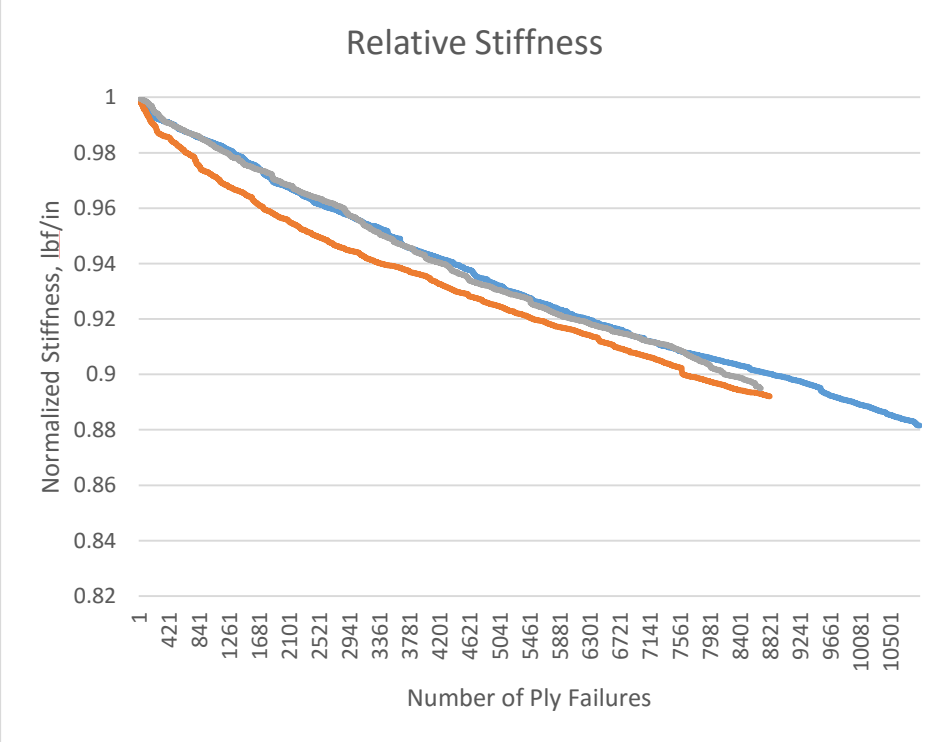

Figure 28: SLA-PD Results, Hexcel BCs, Stiffness Reduction, Normalized

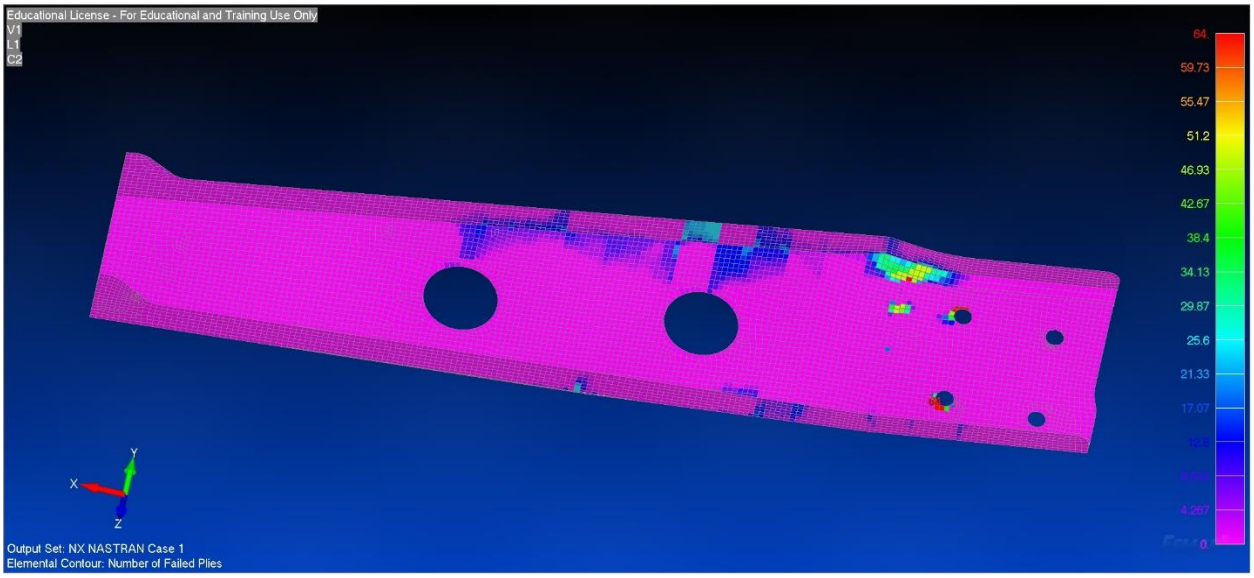

Figure 29: Typical SLA-PD Damage Pattern, Hexcel BCs, 90% Stiffness

Figure 29 shows a typical damage pattern for the Hexcel boundary conditions and the 90% stiffness criterions. Similar to Figure 25, damage is distributed about the model and not localized to one particular area. However in this case, as the analysis was allowed to continue for much longer and many more elements have fully failed, much more damage is visible in the model.

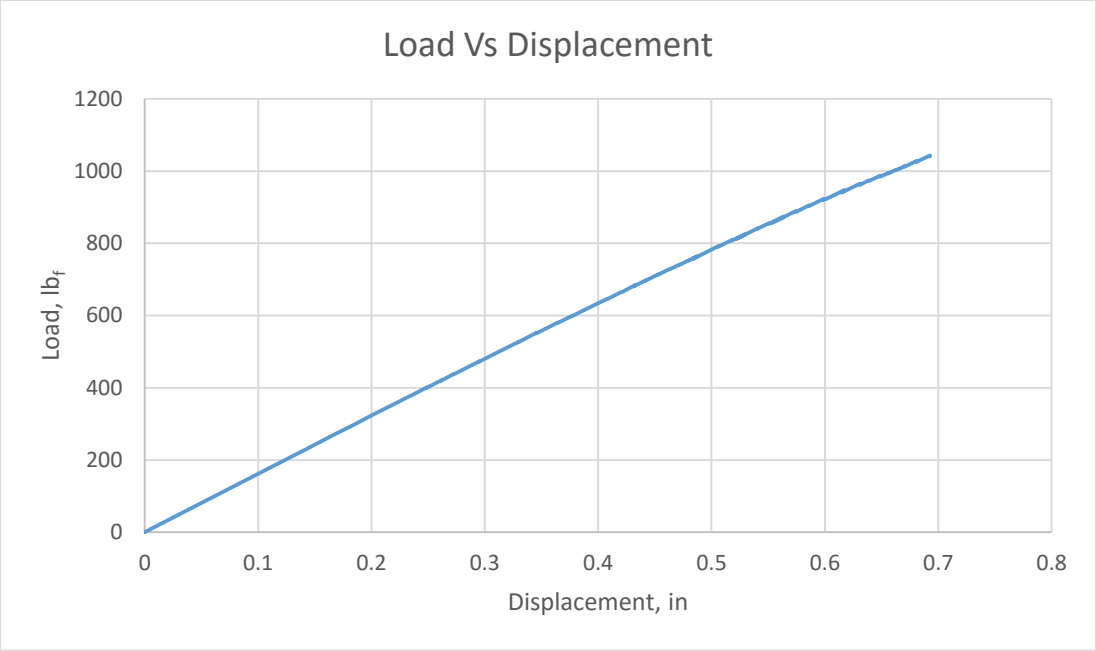

Figure 30: SLA-PD Results, UW BCs, Load vs Displacement, 10% Stiffness Reduction

Figure 30 shows the load displacement relationship for the one completed SLA-PD analysis with UW boundary conditions and the 90% stiffness criterion. Similar to the comparison between Figures 25 and 27, Figure 30 more readily shows non-linear behavior as the load increases. Figure 31 shows the relationship between stiffness and ply failures, and from comparison to Figure 28, it can be seen that relative stiffness decreases by a smaller amount per ply failure than with the Hexcel boundary conditions, and that the analysis time is substantially greater. The former is caused by the different damage patterns between boundary conditions. For the UW analyses, the damage accumulates at the clip end, where each ply failure contributes less to the overall reduction in stiffness than ply failures at the bolt end. Additionally, the longer analysis times are caused by the rigid elements present in the UW model but not the Hexcel model, which increases the time required per iteration.

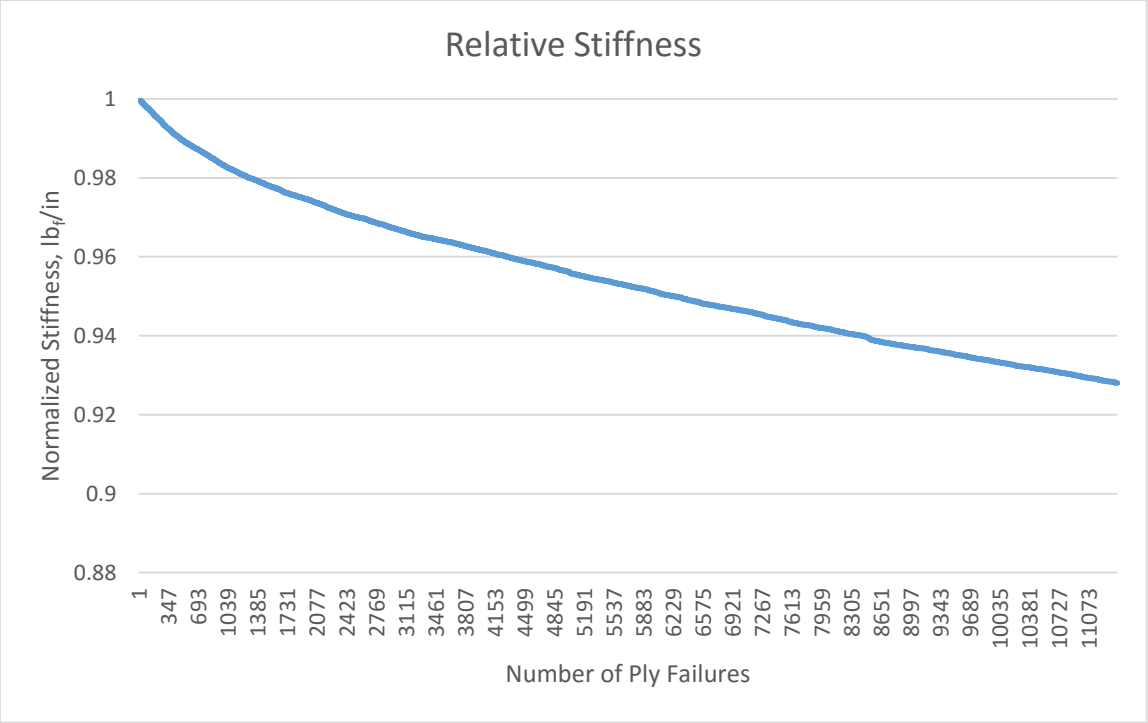

Figure 31: SLA-PD Results, UW BCs, Stiffness Reduction

Figure 32 shows, from top to bottom, the damage pattern resulting from one failed element, from 10 failed elements, and from 90% remaining stiffness. Comparison of the three images shows that while the pattern of damage is generally consistent between them, each successive image shows greatly damage than the previous one. Correspondingly, analysis times increase from image to image, as does the number of element failures, ranging from one, to ten, to upward of 50.

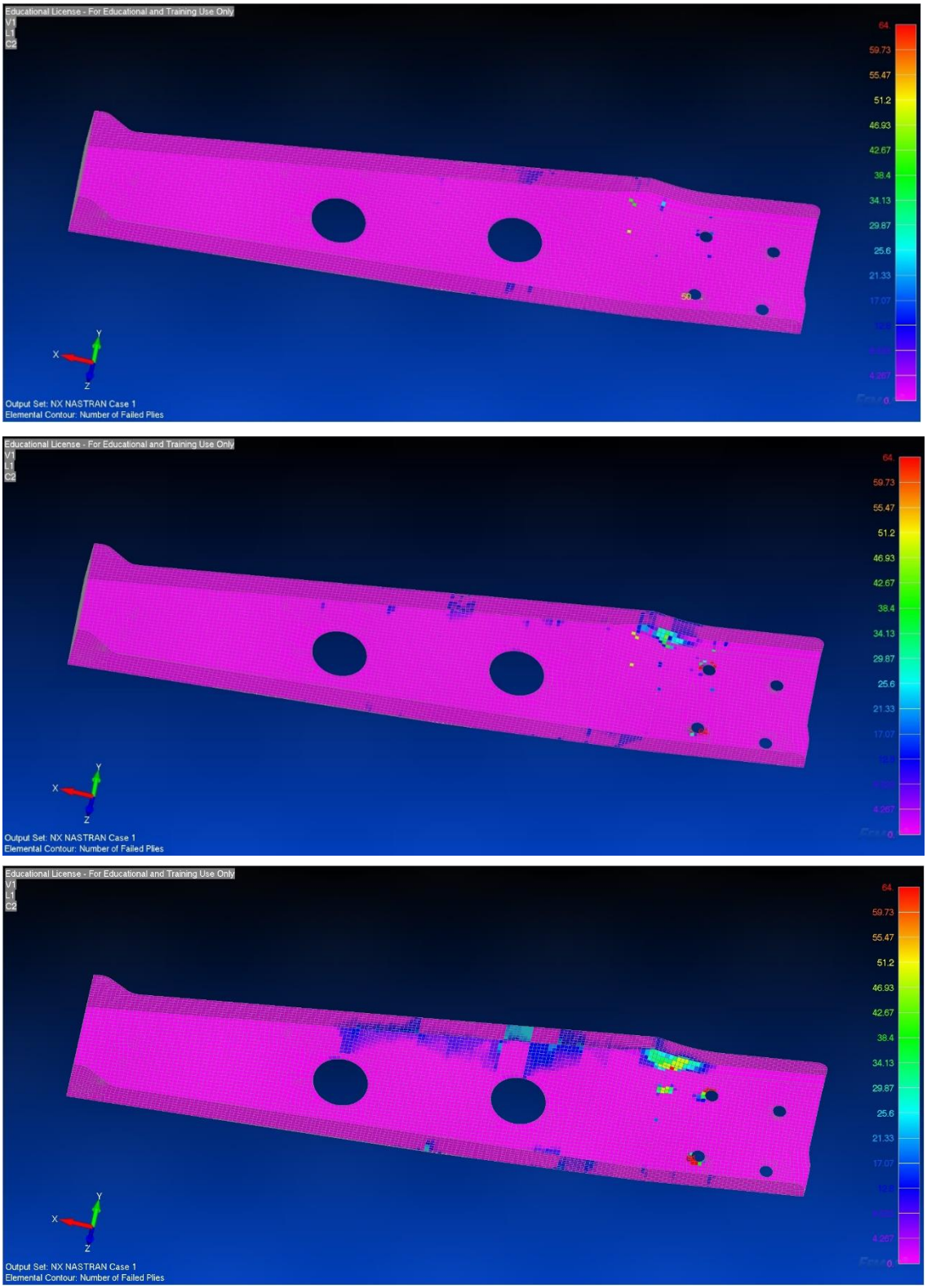

Figure 32: SLA-PD, Typical Damage Patterns, Hexcel BCs, Comparison of Fracture Criterion

Figure 33 shows a damage pattern produced by the UW boundary conditions and the 90% stiffness criterion. As before, damage is heavily concentrated at the clip end, due to the twisting behavior caused by the loading conditions. In this case, some damage is also present in other areas, this is because the teal color on the flanges at the clip end represent full failure of those elements at that thickness. Here as well, the damage is qualitatively consistent with experimental observations in terms of the distribution of damage, and a better match for the amount of damage present in experiments as compared to Figure 24.

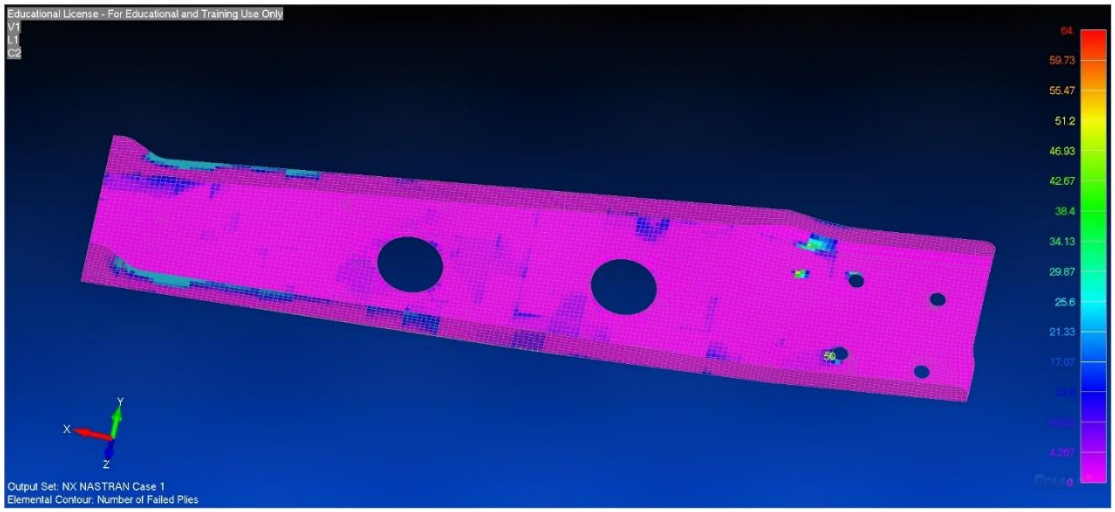

Figure 33: SLA-PD Damage Pattern, UW BCs, 90% Stiffness

9.10 Discussion for 10% Stiffness Reduction

For both sets of boundary conditions, the 90% stiffness criterion correlates better with experimental observations than the other two criterion considered. While promising in that respect, the dramatically increased analysis times call into question the feasibility of this approach with the hardware available for this study.

10. Summary

The techniques developed herein are quite promising with regard to prediction of both the linear and the failure behavior of HexMC. In the linear region, we were able to show that the stochastic laminate analogy produced results that fell within the range predicted by B-Basis deterministic tests, lending credence to existing techniques. This was achieved by applying SLA to a more complex structure than had previously been attempted, as it had previously only been applied to coupon specimens, broadening the viability of the approach.

The combination of SLA with a ply discount scheme resulted in failure predictions that qualitatively matched experiments, even on complex parts. While the computational power available for this study somewhat hampered more robust results, the analyses that were completed indicated promise in predicting the failure behavior of HexMC in various modes of loading.

Taken as a whole, the SLA-PD approach represents a possible avenue of simulating failure within discontinuous fiber composite materials, whereas essentially none existed before.

11. Future Work

While the lengthy analysis times present a significant obstacle, more analyses need to be completed in order to fine tune both the ply discount constants and the structural fracture criterion.

It may be desirable to attempt modeling a simpler structure in order to take advantages of the inherently shorter analysis times involved.

It may also be desirable to perform the linear-elastic SLA analyses again with the new, discounted, properties in order to re-evaluate the distribution of those results within the bracket.

References

1. *Stochastic laminate analogy for simulating the variability in modulus of discontinuous composite materials.* **Feraboli, Paolo et al.** 2010, Composites Part A: Applied Science and Manufacturing.

2. *A Study of Composite Angle Beams Produced using a Discontinuous Fiber Composite.* **Shifman, T. J., & Tuttle, M.** 2011.

3. *Defect and damage analysis of advanced discontinuous carbon/epoxy composite material.* **Feraboli, Paolo et al.** 2010, Composites Part A: Applied Science and Manufacturing. .

4. **Wichita State University.** Composite Materials Handbook -17. [Online] 2013. [Cited: August 21, 2015.] http://www.cmh17.org/.

5. **Head, Brian.** *Analysis Methods for discontinuous fiber composites.* Ann Arbor : University of Washington, Proquest, UMI, 2013.

6. **Hexcel.** HexMC Materials for Industries. *Hexcel Web Site.* [Online] August 29, 2014. [Cited: August 21, 2015.] http://www.hexcel.com/Products/Industries/IHexMC-Materials.

7. **Tuttle, Mark E.** *Structural Analysis of Polymeric Composite Materials Second Edition.* s.l. : CRC Press, 2013. 978-1-4398-7512-4.

8. *A progressive first ply failure model for woven ply CFRP laminates under static and fatigue loads.* **Ch. Hochard, J. Payan, C. Bordreuil.** s.l. : Elsevier Interational Journal of Fatigue, 2006.

9. *Representative volume elements for discontinuous carbon fibre composites – Part 1: Boundary conditions.* **L.T. Harper, C. Qian, T.A. Turner, S. Li, N.A. Warrior.** 2011, Composites Science and Technology.